Progress in Natural Science: Materials International 27 (2017) 297–302

HOSTED BY

Contents lists available at ScienceDirect

Progress in Natural Science: Materials International

journal homepage: www.elsevier.com/locate/pnsmi

Original Research

In-situ secondary growth of nanocube-based Prussian-blue film as an ultrasensitive biosensor

Yu Liu, Jingmeng Peng, Danfeng Jiang, Zhenyu Chu, Wanqin Jin*

State Key Laboratory of Materials-Oriented Chemical Engineering, Jiangsu National Synergetic Innovation Center for Advanced Materials, College of Chemical Engineering, Nanjing Tech University, 5 Xinmofan Road, Nanjing 210009, China

ARTICLE INFO

Keywords:
In-situ secondary growth
Prussian blue film
Regular nanostructure
Electrochemistry
Biosensors

ABSTRACT

A regular nanostructure has been widely confirmed to result ina marked improvement in material performance in biosensing applications. In the present study, a regular nanostructured Prussian blue (PB) film with two heterogeneous crystal layers was synthesized *in-situ* using a secondary growth method. A PB seed layer was first controlled to form uniform cube-like crystal nuclei through an ultrasonic reaction with a single reactant. Then, well-defined 100 nm PB nanocubes were further crystallized on this seed layer using a self-assembly approach. In order to accelerate the electron transfer rate during the enzyme reaction for glucose detection, the graphene was used as the main cross-linker to immobilize glucose oxidase on the PB film. The as-prepared biosensor exhibited high electrocatalysis and electron conductivity for the detection of trace glucose with a sensitivity of 141.5 μA mM^{-1} cm^{-2}, as well as excellent anti-interference ability in the presence of ascorbic acid and uric acid under a low operation potential of −0.05 V.

1. Introduction

In recent decades, biosensor research has achieved significant progress and improvement due to continuously emerging sensing materials. The most important biosensor parameters are sensitivity, selectivity and stability [1–3]. Previously, the scientists believed that the above features were mainly determined by the natural properties of adopted electrode materials [4]. Hence, earlier studies mainly focused on the selection and synthesis of new materials for bioanalysis. However, the current nanomaterial research has demonstrated that the formation of regular nanostructures can greatly improve biosensor performance by promoting catalysis and conductivity [5,6]. Therefore, the design of regular material nanostructures for biosensor fabrication is attracting increasing interest.

Prussian blue (PB), which is known as "artificial peroxidase" [7] due to its excellent electrocatalytic ability for H_2O_2, is used for biosensing analysis of various physiological substances with immobilization of matching oxidases [8]. However, traditional synthesis methods, such as chemical deposition and electrodeposition, cannot harvest PB regular nanostructures due to a fast formation rate which causes excess crystal nuclei and rapid crystallization. In order to resolve this deficiency, Vaucher et al. [9] applied a reverse microemulsion method to obtain regular nanostructured PB powders using an anionic surfactant. Subsequently, Wu et al. [10] developed a sonochemical synthesis route to prepare single-crystalline nanocubic PB crystals with PVP protection. However, these approaches are not able to achieve the *in-situ* formation of regular PB on the electrode surface, which requires an extra immobilization step before application. In our previous studies [11–13], a series of *in-situ* methods were developed to realize the regular growth of PB crystals for performance enhancement. Nevertheless, these structures and the distribution of PB crystals were not integrated and uniform enough, which caused an increase in resistance and a decrease in the catalytic area. Recently, we developed a low-speed chemical synthesis technique to prepare regular PB nanocrystals for a screen-printing ink [14]. Although the geometric structure of the synthesized PB nanocubes was well-defined and uniform, this approach cannot be directly applied to the *in-situ* growth of PB on an electrode. Previous studies [15–17] have shown that the characteristics of a crystal seed determine the crystallization behaviour and the final morphology. PB cannot maintain stability under a high temperature [18], therefore, the widely used hydrothermal synthesis method is not suitable for PB seed formation. In order to obtain a regular and uniform PB film, the seed should be small in size with a uniform distribution. Consequently, the initial stage of PB nucleus formation should be well controlled by the specially designed strategy.

In this study, a uniform PB film with well-defined nanocubic

Peer review under responsibility of Chinese Materials Research Society.

* Corresponding author.
E-mail address: wqjin@njtech.edu.cn (W. Jin).

http://dx.doi.org/10.1016/j.pnsc.2017.04.005
Received 25 October 2016; Received in revised form 5 April 2017; Accepted 10 April 2017
Available online 15 May 2017

crystals was successfully prepared using a secondary synthesis method. A seed layer with 50 nm cube-like PB crystals was first formed by ultrasonic deposition. A self-assembly approach was subsequently used to realize further regular growth of isolated PB crystals 100 nm in size by controlling the assembled layers. Following cross-linking of glucose oxidase by the graphene/glutaraldehyde mixture, the as-prepared biosensor exhibited ultra-sensitivity and excellent anti-interference ability in the detection of glucose under avery low potential.

2. Experimental section

2.1. Reagents and apparatus

Analytic grade $K_4[Fe(CN)_6]\cdot 3H_2O$, $FeCl_3\cdot 6H_2O$, glutaraldehyde, ascorbic acid and uric acid were purchased from Sigma-Aldrich. Five milligrams of glucose oxidase (GOD, EC 1.1.3.4, 168800 units/g, from *Aspergillusniger*, Sigma-Aldrich), 30 wt% H_2O_2 (Sinopharm Chemical Reagent Co., Ltd., Shanghai, China), glucose (Sinopharm Chemical Reagent Co., Ltd.) and graphene powder (Jcnano Technology Co., China) were used directly without purification. All solutions were prepared using deionized water.

The electrochemical tests were performed in 0.1 M PBS at 25 °C using an electrochemical workstation (CHI 660C, Shanghai Chenhua, China). Platinum (Pt) wire and Ag/AgCl were used as the counter and reference electrodes, respectively. The scan rate in cyclic voltammetry (CV) characterization was 50 mV/s. Electrochemical impedance spectroscopy (EIS) measurement of the voltage amplitude at 5 mV in the frequency range 0.05–105 Hz was obtained in the 0.01 M $K_3[Fe(CN)_6]/K_4[Fe(CN)_6]$ solution under an initial potential of 0 V. Online monitoring of PB growth was carried out using a quartz crystal microbalance (QCM200, Stanford Research Systems, Inc., USA). All field emission scanning electron microscopy (FESEM) images were obtained using a Hitachi-4800. An atomic force microscope (AFM) (AFM, XE-100, Park Systems, Korea) was used to obtain information on the morphology of the PB film. The images were collected in non-contact mode.

2.2. Ultrasonic deposition of the PB seed layer

The Au disk electrode (diameter=2 mm) was pretreated with polish and metallographical sandpaper until a mirror-like surface was obtained. The electrode was then washed in deionized water with ultrasonic vibration to remove small residual particles of sandpaper. The electrode was then immersed in the 0.01 M $K_4[Fe(CN)_6]$ solution, and the concentration was changed as necessary. A 25 kHz ultrasonic wave was then used continuously for 1 h. The prepared electrode was then washed with deionized water and dried to complete the process of seed growth.

2.3. Preparation of PB nanocubes by the self-assembly approach

The reactants for PB formation were prepared as follows: solution A, 0.01 M $K_4[Fe(CN)_6]$+0.1 M KCl+0.1 M HCl; solution B, 0.01 M $FeCl_3$+0.1 M KCl+0.1 M HCl. Preparation of each self-assembled layer required four dipping operations of the electrode in solution A, deionized water, solution B and deionized water in turn. The dipping time in solutions A and B was 60 s each time, and the three washing steps in deionized water were set at 15 s each time. Normally, multiple layers were used for preparation of the film.

2.4. Immobilization of glucose oxidase

The enzyme solution was prepared by mixing 5 mg glucose, 5 μL 2% glutaraldehyde solution and 2 mg graphene to 500 μL with phosphate buffer (PBS) solution. For immobilization, 5 μL enzyme solution was placed on each electrode surface and stored at 4 °C for use.

3. Results and discussion

3.1. Formation of the PB seed layer

The PB seed layer requires two functions for biosensor fabrication: one is the provision of growth cores for further crystallization, and the other is the transmission medium for the produced electrons. Seed crystals should be small and have a uniform distribution to provide sufficient space for the regular growth of each PB crystal. The seed layer was formed *in-situ* on the Au electrode by ultrasonic force in $K_4[Fe(CN)_6]$ solution, which relied on the decomposition of $[Fe(CN)_6]^{4-}$ in the acidic solution to produce unbound iron ions [19]. The dissociation of Fe^{2+} from $[Fe(CN)_6]^{4-}$ is usually very slow, but the oxidation of Fe^{2+} is much faster. In terms of reaction kinetics, high molarity of the reactant can accelerate the reaction rate to obtain more products. Therefore, in order to determine the preferred seed layer, the surface morphology and roughness of the electrodes prepared with different $K_4[Fe(CN)_6]$ concentrations were studied using AFM. At the same ultrasonic deposition time, lower concentrations did not easily produce PB crystals, and only a few particles were formed on the supporting electrode (Fig. 1a). When the concentration reached 10 mM, a uniform crystal layer was formed with a roughness of 153 nm (Fig. 1b). However, with further increases in $K_4[Fe(CN)_6]$ concentration, large crystals accumulated together to form an uneven surface at some sites (Fig. 1c and d).

These samples were then characterized by the CV technique to confirm the influence of the seed layer on electrochemical properties (Fig. 2). It was found that the current value of redox peaks was enhanced with increased $K_4[Fe(CN)_6]$ concentration which was attributed to the increased coverage of PB seeds. In addition, the potential difference of redox peaks, which can indicate the strength of electron transfer resistance [20], were calculated to be 41, 38, 90 and 71 mV for the electrodes prepared under 5, 10, 30 and 50 mM $K_4[Fe(CN)_6]$, respectively. When considering the above AFM characteristics, these results demonstrated that 0.01 M $K_4[Fe(CN)_6]$ reactant was the optimum condition for synthesizing a uniform PB seed layer with low electron transfer resistance for ultrasonic deposition.

3.2. The influence of self-assembled layers

Following preparation of the seed layer, further synthesis of the PB film was performed to realize regular growth. Self-assembly is a multilayer fabrication approach [21], the film morphology, coverage

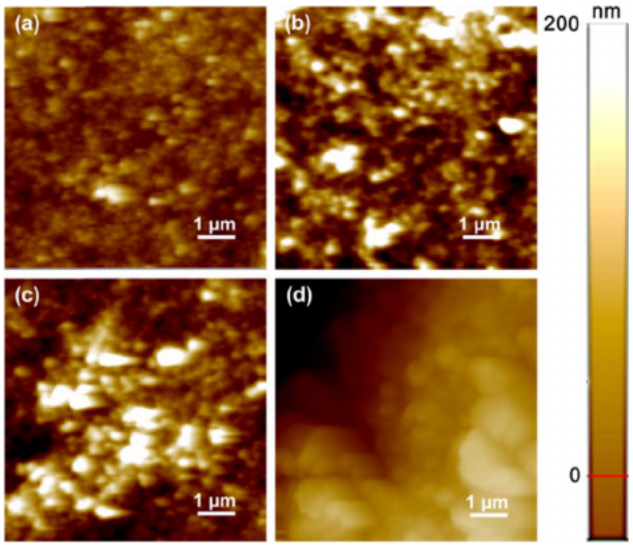

Fig. 1. AFM images of seed layers prepared using different reactant concentrations: (a) 5 mM; (b) 10 mM; (c) 30 mM; (d) 50 mM.

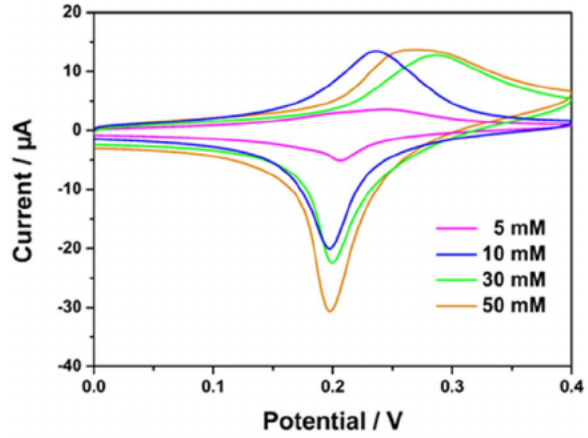

Fig. 2. CV diagrams of PB seed layers prepared with different $K_4[Fe(CN)_6]$ concentrations using the ultrasonic deposition method.

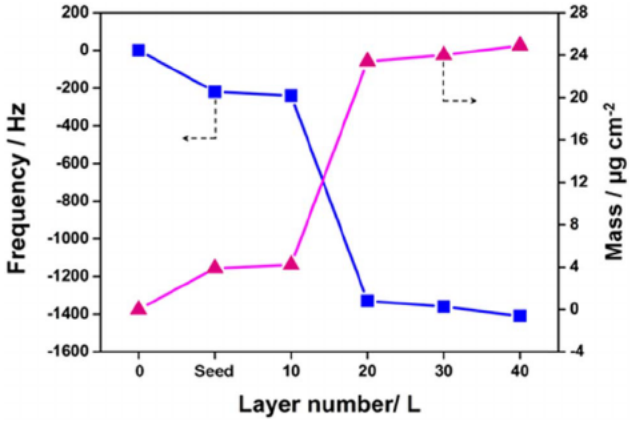

Fig. 3. Mass of PB films with different assembled layers detected using a quartz crystal microbalance.

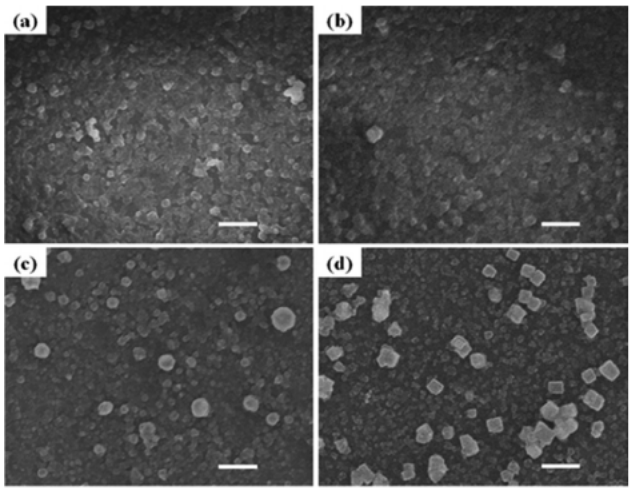

Fig. 4. FESEM images of PB films prepared with (a) the seed layer and self-assembled (b) 10, (c) 20, (d) 40 layers. The bar is 200 nm.

and thickness can be precisely managed by the assembled layers. In order to control the preparation process, a quartz crystal microbalance (QCM) was used to monitor the coverage mass of the PB film due to the increase in deposition layers. The vibration frequency of the Au quartz disk showed a continuous decrease confirming the increase inmass according to the following equation [22]:

$$\Delta f = -C_f \times \Delta m \quad (1)$$

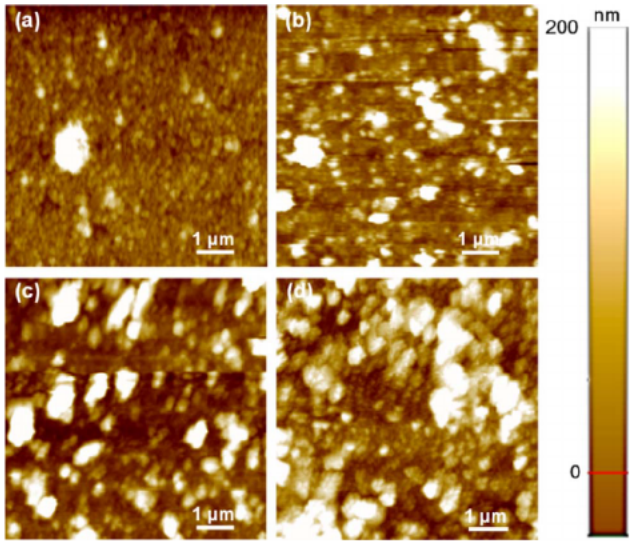

Fig. 5. AFM results of PB films prepared with (a) the seed layer and self-assembled (b) 10, (c) 20, (d) 40 layers.

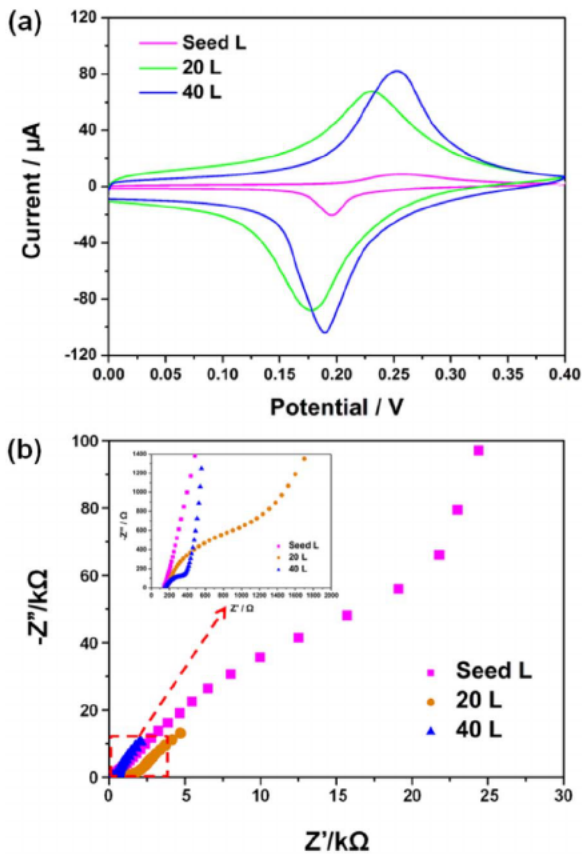

Fig. 6. (a) CV diagrams of PB films prepared by the seed, 20 and 40 assembled layers; (b) EIS results of PB films prepared by the seed, 20 and 40 assembled layers. The inset shows the magnified image of the high frequency region.

where Δf is the frequency change in Hz; Δm is the change in mass per unit area; C_f is the sensitivity factor for the crystal (56.6 Hz g^{-1} cm^2).

According to Fig. 3, ultrasonic deposition was confirmed as an efficient method for PB synthesis. The PB coverage mass prepared by ultrasonic deposition was much higher than the self-assembly approach up to 10 layers of deposition. In assemblies with 10–20 layers, a sudden increase in the amount of PB was observed. This phenomenon was further investigated by FESEM to characterize electrode samples of only the seed layer, and of 10, 20 and 40 assembled layers. It can be

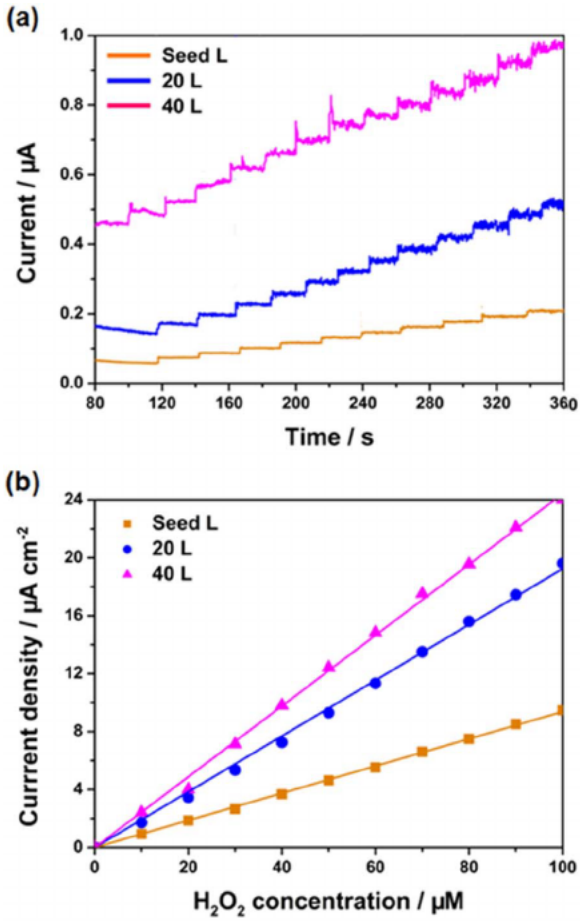

Fig. 7. (a) Chronoamperometry of PB films with the seed layer, 20 and 40 self-assembled layers in relation to H_2O_2 response. (b) Linear calibration of the relationship between current density and H_2O_2 concentration.

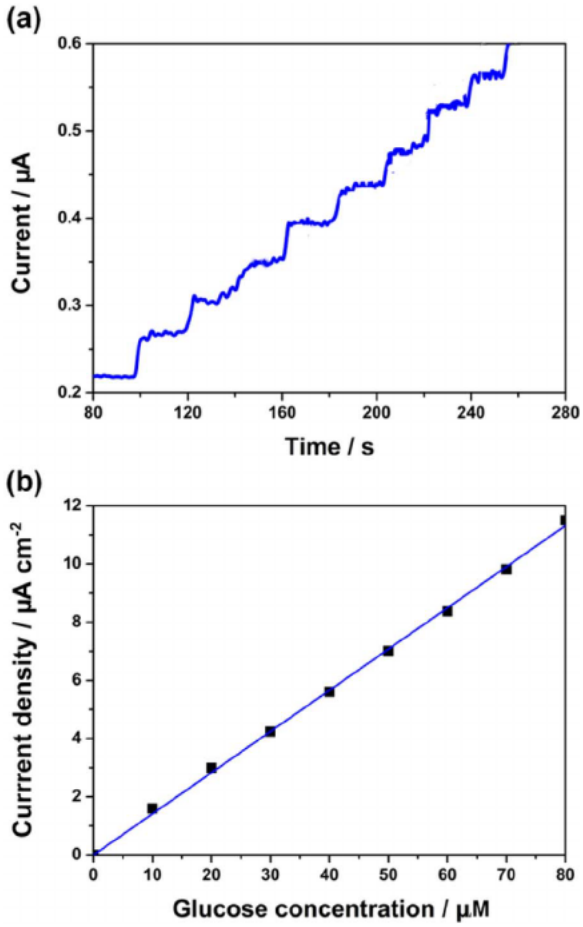

Fig. 8. (a) Chronoamperometry diagram of the PB nanocubes-based biosensor for glucose detection. (b) Linear calibration of chronoamperometry data.

seen that after modification of the PB seeds, the electrode surface was almost covered with small PB particles (Fig. 4a). Numerous crystals formed the cube-like shape which was approximately 50 nm in size. However, the first 10 assembled layers did not produce obvious changes in surface morphology, and only the seed size was larger (Fig. 4b). However, the next 10 layers not only filled the deficiencies which were uncovered by the seeds, but also formed many isolated large crystals with irregular structures on the seed layer (Fig. 4c). Up to 40 layers deposition, numerous well-defined nanocubes were synthesized on the top of the seed layer (Fig. 4d). The size of each cube was only 100 nm and showed excellent ability to control the self-assembly approach to decrease the crystallization rate. The effect of different assembly layers on film thickness was further investigated by AFM. As shown in Fig. 5, PB film thickness continuously increased with an increase in deposition layer. From the seed layer to 40 assembled layers, the average thickness of the films was calculated to be110, 132, 156, 181 nm, respectively. The size of each PB crystal increased, but rare aggregation occurred which changed the cubic shape.

It has been demonstrated that a change in material morphology often affects performance [23–25]. Therefore, the electrochemical properties of synthesized films with different structures were further analysed by CV scanning. In addition to the electrocatalysis current, the potential difference between the oxidation and reduction peaks also changed with different film features. The exact potential differences were calculated to be 70, 56 and 62 mV for the seed, 20 and 40 assembled layer films, respectively (Fig. 6a). Thus, the formation of nanocubes caused a slight decrease in reaction reversibility compared with irregular crystals, but was still better than the seed layer. However, it should be noted that the current peak value was highest for the 40 layer film, which demonstrated superior electrocatalysis of PB regular nanocubes compared with irregular crystals.

For clarity, the same samples were then investigated by EIS (Fig. 6b). Through the simulation of an equivalent circuit [26], the seed layer exhibited the largest interface resistance for electron transfer. This was because the seed layer was composed of numerous independent nanoparticles which easily formed film defects. The gaps between each crystal can cause signal interruptions which greatly increase resistance for electron transfer. Interface resistance of the films with 20 and 40 layers was calculated to be 2456.7 and 508.8 Ω, respectively, using the fitted Nyquist curves [27]. This indicated that the gaps in the seed layer were continuously filled with the increasing deposition layers. In the 40 layer assembly, the top regular crystals enhanced the contact area promoting electron transfer from the electrolyte to the substrate electrode.

3.3. Biosensing performance of the nanocubic PB film

The relationship between regular structure and performance of the prepared PB films was studied by chronoamperometry. Due to the direct electrocatalytic ability of PB, H_2O_2 first served as the target for characterization. The sensing performance of the seed layer, 20 and 40 layer assembled films, which had different surface structures and preparation stages, was measured under a steady −0.05 V. After addition of the same concentration of H_2O_2, all films immediately produced a stable current step and showed a rapid response to H_2O_2. With continuous additions, the neighbouring current steps were clearly seen to exhibit a good linear correlation (Fig. 7a). The relationships between the response currents and H_2O_2 concentrations were used as

Table 1
Comparison of the performance of reported glucose biosensors.

Materials	Potential (V)	Sensitivity (μA mM^{-1} cm^{-2})	Limit of detection (μM)	Linear range (nM)	References
PB nanocubes	−0.05	141.5	10	0.001–0.8	This work
PB nanogrid	−0.1	34.8	200	0.002–1.5	[8]
GNS-PEI-AuNPs	0.35	93	0.32	0.001–0.1	[30]
GCE/rGO-Ni/Chitosan	0.25	129	390	0.025–1	[31]
Pt/GO	0.4	8	–	0.1–20	[32]
PDDA-AuNPs/MWCNTs	−0.45	29.72	4.8	0.005–0.175	[33]
GCE/rGO	−0.44	1.85	–	0.1–27	[34]
n-TiO_2/PANI	−0.45	6.31	18	0.02–6	[35]
RGO/Ag	−0.49	3.84	160	0.5–12.5	[36]
CuS/CS/GCE	0.46	5.86 (μA mM^{-1})	0.3	0.001–1	[37]

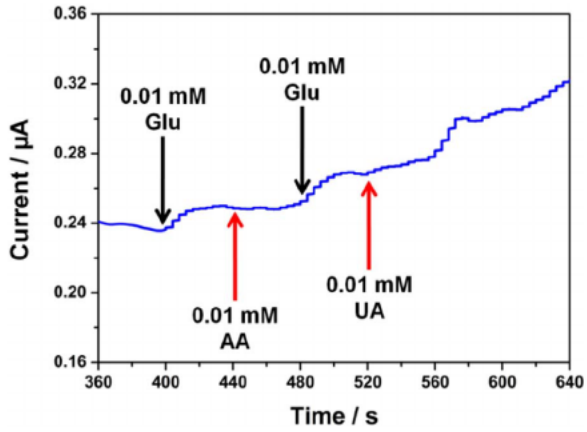

Fig. 9. Anti-interference of the prepared glucose biosensor.

the calibration diagrams in Fig. 6b. By linear fitting, the sensitivities of the PB films were calculated to be 78.2, 192.4 and 244.4 μA mM^{-1} cm^{-2} for the seed layer, 20 and 40 assembled layers respectively. These results revealed that the seed layer partially contributed to the electrocatalysis of the PB nanocubes-based film. Hence, the main catalytic activity was attributed to the upper nanocubes, indicating that regularization of material structure benefitted performance.

Before glucose detection, the glucose oxidase is required to be immobilized on the film surface. The most widely applied technique is the glutaraldehyde (GA) cross-linking method [28]. However, the presence of GA can affect the electron transfer due to its weak conductivity [29], although it can firmly lock the enzyme on the electrode surface. Accordingly, graphene was mixed with the prepared enzyme solution to improve conductivity for enzyme immobilization. The performance of the as-prepared enzymatic biosensor was then investigated. As shown in Fig. 8a, each addition of 10 μM glucose produced an obvious current step, although some signal noise occurred. The response period of each addition was less than 5 s and showed the fast enzyme reaction and electron transfer rates of the prepared biosensor. According to these data, the sensitivity of the PB nanocubes-based biosensor was 141.5 μA mM^{-1} cm^{-2} for glucose detection after calibration.

We compared the performance of this biosensor with that of previously reported glucose biosensors. As shown in Table 1, the sensitivity level was much higher than most recently reported biosensors. Although the applied material was the same as that in our previous work [8], the nanocube structure was four times more sensitive than the nanogrid shape. This was mainly due to the high catalytic activity of regular edges in the cubic geometry. It should be noted that this excellent sensitivity was obtained under a low potential, which can promote the anti-interference ability in practical applications. According to the data listed in Table 1, graphene or reduced graphene oxide film can be operated at −0.45 or lower, however, the sensitivities of these materials are unsatisfactory. In the present study, compared with H_2O_2 detection, the detection of glucose undergoes an extra enzyme reaction which could cause a marked decrease in the efficiency of electrocatalysis and conductivity. However, for our prepared biosensor, the decrease was less than two-fold and the biosensor exhibited high catalysis and low resistance due to the nanocubes and graphene mixed enzyme layer.

Due to the complicated composition in a real system, such as blood, the accuracy of the output signal is an essential parameter in biosensing. Normally, ascorbic acid (AA) and uric acid (UA), which are easily oxidized under high potential [38], often coexist with glucose. Hence, they served as interferences to examine the anti-interference ability of the as-prepared biosensor. In this experiment, the same concentration of AA or UA was respectively added to the detection system after each glucose addition. The results (Fig. 9) showed there was no obvious current change compared with the glucose response. This good selectivity was mainly attributed to the low working potential of the prepared PB biosensor which was much lower than the oxidation potential of both AA and UA [39,40].

4. Conclusions

In this study, we have fabricated *in-situ*a nanocube-based PB film with two heterogeneous nanocrystal layers using a secondary growth approach which integrates ultrasonic deposition and self-assembly methods. The bottom layer of this film is a seed layer with densely accumulated 50 nm cube-like crystals, and the top layer is composed of uniformly distributed nanocubes 100 nm in size. The as-prepared biosensor exhibited high sensitivity and selectivity for the detection of glucose under very low potential of −0.05 V. This *in-situ* secondary synthesis strategy of structure control is promising and could be further applied in the more regular nanostructures of electrode materials, and our prepared biosensor with high performance can be used to analyze other physiological activators by changing the oxidase.

Acknowledgements

This work was supported by the Innovative Research Team Program of the Ministry of Education of China (No. IRT13070), the Jiangsu Province Natural Science Foundation for the Youth (No. BK20140931) and Top-notch Academic Programs Project of Jiangsu Higher Education Institutions (TAPP).

References

[1] M. Yang, Y. Yang, B. Liu, G. Shen, R. Yu, Sens. Actuators B Chem. 101 (2004) 269–276.
[2] C. Nistor, J. Emneus, L. Gorton, A. Ciucu, Anal. Chim. Acta 387 (1999) 309–326.
[3] Z. Chu, L. Shi, Y. Liu, W. Jin, N. Xu, Biosens. Bioelectron. 47 (2013) 329–334.
[4] A. Sarma, P. Vatsyayan, P. Goswami, S. Minteer, Biosens. Bioelectron. 24 (2009) 2313–2322.

[5] P. Solanki, A. Kaushik, V. Agrawal, B. Malhotra, NPG Asia Mater. 3 (2011) 17–24.
[6] S. Roy, Z. Gao, Nano Today 4 (2009) 318–334.
[7] A. Karyakin, E. Karyakina, L. Gorton, Anal. Chem. 72 (2000) 1720–1723.
[8] Z. Chu, L. Shi, Y. Zhang, W. Jin, S. Warren, D. Ward, E. Dempsey, J. Mater. Chem. 22 (2012) 14874–14879.
[9] S. Vaucher, M. Li, S. Mann, Angew. Chem. Int. Ed. 38 (2000) 3680–3738.
[10] X. Wu, M. Cao, C. Hu, X. He, Cryst. Growth Des. 6 (2006) 26–28.
[11] Z. Chu, Y. Zhang, X. Dong, W. Jin, N. Xu, B. Tieke, J. Mater. Chem. 20 (2010) 7815–7820.
[12] Z. Chu, L. Shi, Y. Liu, W. Jin, N. Xu, J. Mater. Chem. 21 (2011) 11968–11972.
[13] Y. Zhang, Y. Liu, Z. Chu, L. Shi, W. Jin, Sens. Actuators B Chem. 176 (2013) 978–984.
[14] D. Jiang, Z. Chu, J. Peng, W. Jin, Sens. Actuators B Chem. 228 (2016) 679–687.
[15] M. Mahmoud, M. El-Sayed, J. Gao, U. Landman, Nano Lett. 13 (2013) 4739–4745.
[16] G. Coquerel, Chem. Soc. Rev. 43 (2014) 2286–2300.
[17] H. Li, W. Fan, B. Peng, W. Wang, Y. Zhuang, L. Guo, X. Yao, H. Ikuta, Cryst. Growth Des. 15 (2015) 1740–1744.
[18] Q. Wu, G. Wu, L. Wang, W. Hu, H. Wu, Mater. Sci. Semicond. Proc. 30 (2015) 476–481.
[19] Y. You, X. Wu, Y. Yin, Y. Guo, Energy Environ. Sci. 7 (2014) 1643–1647.
[20] C. Hu, T. Tsou, Electrochem. Commun. 4 (2002) 105–109.
[21] R. Millward, C. Madden, I. Sutherland, R. Mortimer, S. Fletcher, F. Marken, Chem. Commun. (2001) 1994–1995.
[22] S. Diltemiz, D. Hur, A. Ersoz, A. Denizli, R. Say, Biosens. Bioelectron. 25 (2009) 599–603.
[23] J. Romo-Herrera, M. Terrones, H. Terrones, S. Dag, V. Meunier, Nano Lett. 7 (2007) 570–576.
[24] M. Daniel, D. Astruc, Chem. Rev. 104 (2004) 293–346.
[25] S. Arya, S. Saha, J. Ramirez-vick, V. Gupta, S. Bhansali, S. Singh, Anal. Chim. Acta 737 (2012) 1–21.
[26] J. Garcia-Jareno, J. Navarro, A. Roig, H. Scholl, F. Vicente, Electrochim. Acta 40 (1995) 1113–1119.
[27] X. Luo, J. Xu, Q. Zhang, G. Yang, H. Chen, Biosens. Bioelectron. 15 (2005) 190–196.
[28] F. Richards, J. Knowles, J. Mol. Biol. 37 (1968) 231–233.
[29] A. Harreveld, F. Khattab, J. Cell Sci. 3 (1968) 579–594.
[30] P. Rafighi, M. Tavahodi, B. Haghighi, Sens. Actuators B Chem. 232 (2016) 454–461.
[31] R. Krishna, J.M. Campina, P.M.V. Fernandes, J. Ventura, E. Titus, A.F. Silva, Analyst 141 (2016) 4151–4161.
[32] Y. Liu, D. Yu, C. Zeng, Z. Miao, L. Dai, Langmuir 26 (2010) 6158–6160.
[33] Y. Yu, Z. Chen, S. He, B. Zhang, X. Li, M. Yao, Biosens. Bioelectron. 52 (2014) 147–152.
[34] B. Unnikrishnan, S. Palanisamy, S. Chen, Biosens. Bioelectron. 39 (2013) 70–75.
[35] W. Tang, L. Li, X. Zeng, Talanta 131 (2015) 417–423.
[36] S. Palanisamy, C. Karuppiah, S. Chen, Colloid Surf. B 114 (2014) 164–169.
[37] Y. Yang, J. Zi, W. Li, Electrochim. Acta 115 (2014) 126–130.
[38] K. Lin, T. Tsai, S. Chen, Biosens. Bioelectron. 15 (2010) 608–614.
[39] Z. Wang, J. Liu, Q. Liang, Y. Wang, G. Luo, Analyst 127 (2002) 653–658.
[40] R. Wang, H. Qun, Li, Biosens. Bioelectron. 21 (2006) 1086–1092.